ORIGINAL PAPER

Developing science-informed maps and climate service for extreme rainfall in Spain

S. M. Vicente-Serrano[1,2] (ORCID) · **S. Beguería**[3,2] · **F. Reig**[1,2] · **A. Royo**[1,2] · **M. Arretxea**[4] ·
M. Gil[3,2] · **B. Latorre**[3,2] · **A. El Kenawy**[1,2] · **M. Franquesa**[1,2] · **A. Halifa-Marin**[1,2] ·
M. Adell-Michavila[1,2] · **A. Crespillo**[1,2] · **D. Pérez-Pajuelo**[1,2] · **F. Domínguez-Castro**[1,2] ·
D. Barriopedro[4] · **J. M. Gutiérrez**[5] · **C. Azorin-Molina**[6] · **L. Gimeno**[7,8,9] · **R. Nieto**[7,8,9]

Abstract

This study introduces the first high-resolution hazard probability maps of extreme precipitation for Spain, marking a significant step toward a national climate service for hydrometeorological extremes. Using long-term daily precipitation records from a dense network of stations and incorporating topographic data, the methodology combines the Generalized Pareto distribution with universal kriging to spatially interpolate distribution parameters. These maps offer reliable estimates of extreme precipitation quantiles, validated against station-level observations, and are based on a stationary modelling framework—an approach supported by recent findings showing the temporal stability of such extremes in Spain and considered more robust than non-stationary alternatives. Distinct spatial patterns emerge, with intense daily precipitation distributed mainly along the Mediterranean coast and high total event precipitation in the northwest and southwest, reflecting the influence of varied weather systems. To support decision-making, the study aggregates these high-resolution data at the provincial level, aligning risk information with administrative boundaries, and enhancing its relevance for policy and planning. Furthermore, the maps are made accessible via an interactive online platform (https://retornolluvias.csic.es), enabling users to explore localized hazard probabilities, thereby supporting adaptation in water management and civil protection, among others.

Keywords Extreme precipitation · Hazard probability maps · Spatial interpolation · Stationary models · Climate services

1 Introduction

Extreme precipitation events are a primary driver of erosion processes, soil loss, and increased risks of land degradation and desertification (Mulligan 1998; Yao et al. 2020). They also significantly impact land stability, often triggering mass movements such as landslides and debris flows (Kirschbaum et al. 2012, 2020). Further, extreme precipitation is

---

the main factor behind floods of various types. Flash floods typically result from intense precipitation occurring over a short period (Norbiato et al. 2007; Smith et al. 2019), while river floods are driven by prolonged heavy rainfall, which affects large areas and accumulates within river systems (Tarasova et al. 2019). These events lead to severe infrastructure damage, including the destruction of dams, roads, and other critical structures (Peng and Zhang 2012; Singh et al. 2018). They also disrupt economic activities, such as agriculture and industry (Merz et al. 2010; Lesk et al. 2016), and, most critically, cause profound social consequences, including the loss of homes and human lives (French et al. 1983; Jonkman 2005; Ebi et al. 2020).

Globally, climate model studies suggest that the frequency of extreme precipitation events could increase under global warming scenarios (Papalexiou and Montanari 2019; Myhre et al. 2019; Li et al. 2021). Moreover, observational studies indicate that such changes are already occurring in many regions of the world (Donat et al. 2014; Seneviratne et al. 2021). In the Mediterranean Basin, and particularly in Spain, existing studies do not provide clear evidence of an increase in extreme precipitation events (Acero et al. 2011; Serrano-Notivoli et al. 2018; Beguería et al. 2025). In fact, the latest IPCC report assigns low confidence to trends related to extreme precipitation in the Mediterranean region (Seneviratne et al. 2021), as precipitation in this area is characterized by strong interannual and decadal variability (Vicente-Serrano et al. 2025). Nevertheless, precipitation patterns in this region exhibit significant spatial variability, with some areas experiencing very humid conditions, and others approaching an arid climate. This is particularly true for Spain, a country frequently affected by extreme precipitation events, though with considerable regional differences in their magnitude (Beguería et al. 2009; Cortesi et al. 2014; Domínguez-Castro et al. 2019).

Given the significant impacts of extreme precipitation events and their strong spatial variability, it is essential to establish accurate spatial estimations of precipitation hazard probability (Nerantzaki and Papalexiou 2022). Such estimations provide crucial information for developing effective territorial planning strategies that integrate precipitation hazard considerations into environmental, economic, and social management, including civil protection mechanisms. Various approaches have been employed to estimate the probability of precipitation events of different intensities and durations using long-term meteorological station records (Milojevic et al. 2023; Anzolin et al. 2024; Koutsoyiannis et al. 2024; Billios and Vasiliades 2025). Additionally, some methodologies extend these point-based estimations to ungauged areas by regionalization approaches (Haruna et al. 2022) and spatial interpolation of station data. There are previous developments of maps of extreme precipitation hazard based on the application of extreme value theory analysis and spatial interpolation techniques in some regions like Greece (Iliopoulou et al. 2024), Argentina (Catalini et al. 2021), Germany (Miniussi and Marra 2021), United States (Risser et al. 2019), and regions of Italy (Formetta et al. 2024), China (Zou et al. 2021), Sweden (Ul Hassan et al. 2021), Slovakia (Szolgay et al. 2009), Spain (Beguería et al. 2009) and northern Algeria (Meddi and Toumi 2015), among others. These hazard probability maps offer valuable insights into the likelihood of precipitation events of varying intensity and duration, supporting informed decision-making in risk management and planning.

These maps may be affected by uncertainties if the precipitation records are short (Serinaldi and Kilsby 2014), or if they are characterized by a sparse distribution of meteorological stations or by the presence of complex topographic features that complicate detailed estimations (Mascaro 2018). They may also be affected by uncertainties arising from the potential

non-stationary behavior of extreme precipitation events (Luke et al. 2017; Anzolin et al. 2024; Beguería et al. 2025), which could limit the representativeness of extreme precipitation quantiles in a changing climate.

In this study, we develop for the first time maps of extreme precipitation quantiles for Spain as a basis for generating an interactive climate service that allows users to access precipitation quantiles for extreme events. To reduce existing uncertainties, we have carefully processed all available daily precipitation data in Spain to ensure both a high density of stations—necessary to cover the region's geographic diversity—and sufficiently long-term records to provide a representative and accurate assessment of extreme precipitation hazard probabilities.

2 Data and methods

2.1 Database

We used data from 2,840 daily precipitation stations for 1961–2024 (Fig. 1). Those stations were selected from the complete set of daily precipitation records available from the Spanish Meteorological Agency (AEMET), which includes raw data from almost 11,000 stations. This dataset underwent rigorous quality control (Vicente-Serrano et al. 2010), and series containing more than 35 years of original data were reconstructed using a quantile matching approach based on neighboring stations (Beguería et al. 2019). For this recon-
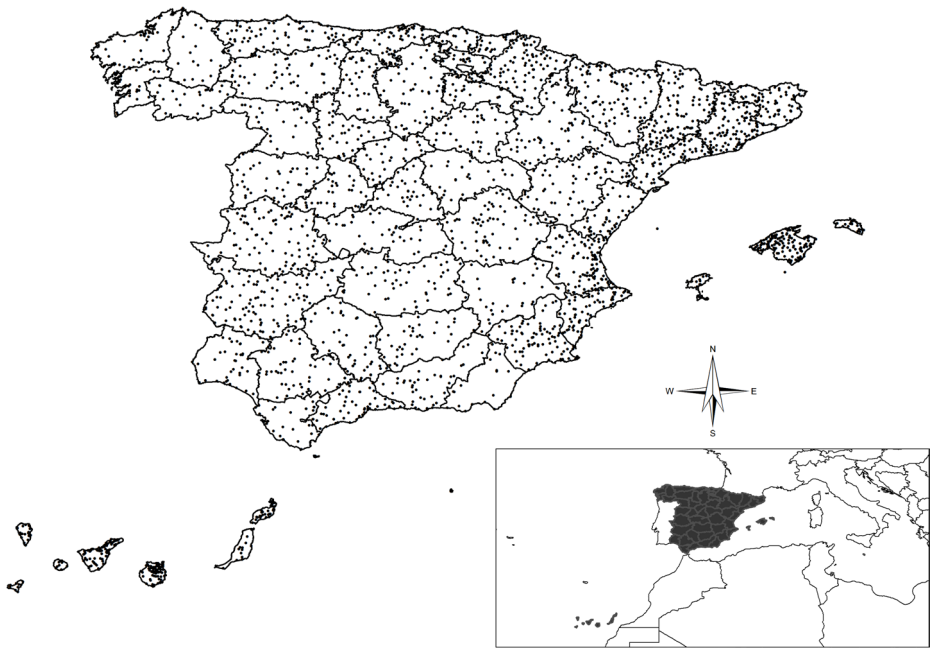

Fig. 1 Spatial distribution of the daily precipitation stations used in this study. The limits represent the Spanish provinces

struction, only series with at least a 15-year overlap and located within a 50 km radius of the target station were considered (see further details in Beguería et al. 2025).

2.2 Methods

2.2.1 Selection of the sample

This study followed the methodological approach described by Beguería and Vicente-Serrano, (2006), with some modifications. We focus on estimating the pointwise hazard probability across Spain of two different variables: the maximum daily precipitation recorded during an event of consecutive precipitation days, and the total precipitation accumulated over these consecutive days. These two variables are relevant for assessing the risk of flash floods in the first case, and the occurrence of river floods and landslides in the second (Braud et al. 2016; Seneviratne et al. 2021). To ensure the independence of the analyzed records, we selected the maximum daily precipitation recorded during each event.

We used extreme value theory to estimate the probability of events exceeding a specified threshold (Hershfield 1973). For this purpose, we followed the partial duration (PD) series approach, which involves defining a threshold and selecting only the values that exceed it. These exceedances, denoted as y, are the values above the chosen threshold. As previous studies have shown that optimal threshold values can vary globally depending on climatic characteristics (Wang et al. 2020), we tested several methods to define the threshold for selecting the exceedance series. On one hand, we used percentile-based thresholds, specifically the 90th, 92.5th, and 95th percentiles. On the other hand, we applied alternative threshold estimation methods included in the tea R package (https://cran.r-project.org/web/packages/tea/tea.pdf), such as the Hill estimator and single and double bootstrap procedures for determining the optimal sample fraction (Hall and Welsh 1985; Caeiro and Gomes 2014).

2.2.2 Quantile estimation

The series of exceedances over a threshold tend to converge to a Generalized Pareto Distribution (GPD) (Pickands III, 1975), a behavior that has been observed in extreme precipitation series (Gamet and Jalbert 2022). The GPD is characterized by three parameters: the origin parameter (x_0), the shape parameter (κ) and the scale parameter (α). Its cumulative distribution function (CDF) is given by:

$$P\left(Y \leq y | \alpha, \kappa\right) = 1 - \left(1 - \kappa \frac{y}{\alpha}\right)^{\left(\frac{1}{\kappa}\right)}, (y_i = x_i - x_0).$$

In this study, the parameters of the GPD were estimated using the method of probability-weighted moments (Hosking and Wallis 1987), which has been shown to provide reliable estimates for fitting precipitation data (Nerantzaki and Papalexiou 2022).

The probability of an exceedance Y is commonly expressed in terms of its return period t, defined as the expected time between two consecutive occurrences of the event. The return period is the inverse of the probability of exceedance. For a given threshold exceedance y, the return period over t years is calculated as:

$$t_y = \frac{1}{\lambda\left[1 - P\left(Y \le y\right)\right]}$$

where λ is a frequency parameter representing the average number of occurrences of Y per year in the sample. Alternatively, the return level (or maximum value expected) *E* in a period of *t* years is given by:

$$E_y\left(t\right) = x_0 + \frac{\alpha}{\kappa}\left[1 - \left(\frac{1}{\lambda t}\right)^k\right]$$

Regarding the potential non-stationary behavior of extreme precipitation, it is important to highlight that recent studies have indicated that such events in Spain are largely stationary (Beguería et al. 2025), supporting the use of a stationary approach in this study. Moreover, stationary approaches are more reliable and yield smaller uncertainty than non-stationary ones (Serinaldi and Kilsby 2015).

Therefore, three parameters of the GPD were estimated at each of the 2,840 meteorological stations employed in this study, and for each variable of interest separately. This procedure enabled the determination of the return period corresponding to a given maximum intensity and total magnitude of precipitation for a specific event and location. The uncertainty of these estimates strongly depends on the sample size, with greater uncertainty typically associated with the highest values. Therefore, the magnitude-frequency curves must be accompanied by estimates of their corresponding confidence intervals, which were defined according to Rao and Hamed (2000).

2.2.3 Spatial mapping

Several studies have recommended adopting a regionalization approach to estimate spatial variations in the probability of extreme precipitation events over large areas (Khalili et al. 2011; Haruna et al. 2022; Alshehri et al. 2024). This method identifies common distribution parameters within specific regions. However, limitations exist in areas with complex terrain or high spatial variability in extreme events. In such regions, regionalisation struggles to capture local precipitation characteristics, especially where significant spatial shifts in distribution parameters occur (Deidda et al. 2021). Such an issue highlights the advantages of spatial interpolation methods for estimating high return period quantiles (Claps et al. 2022).

While some studies have directly interpolated extreme precipitation quantiles (Meddi and Toumi 2015; Das 2019; Zou et al. 2021; Miniussi and Marra 2021), interpolating the parameters of the underlying probability distribution has been shown to perform significantly better (Yin et al. 2018; Das et al. 2020). This approach also provides the flexibility needed to develop interactive maps and services for estimating extreme events.

Following previous research (Beguería and Vicente-Serrano 2006; Yin et al. 2018; Iliopoulou et al. 2024; Formetta et al. 2024), we applied an approach to map the parameters of the fitted distributions at a spatial resolution of 2.5 km, enabling estimation in areas without direct observations. This allows return periods associated with selected maximum and total precipitation magnitudes over the events to be determined at any location in Spain.

To interpolate the distribution parameters x_0, α, κ and λ, we used the universal kriging algorithm. Unlike ordinary kriging, which assumes a constant mean across space, universal kriging models the mean as a deterministic function of spatial coordinates, typically using a polynomial trend surface (Burrough and McDonnell 1998; Pebesma 2004). This method incorporates large-scale trends along with local spatial correlation captured by the variogram. The algorithm consists of two main steps: first, estimating the underlying spatial trend using a regression model; second, interpolating the spatially correlated residuals using kriging. This dual-step process allows for both global patterns and local dependencies to be addressed, making universal kriging especially suitable for environmental and meteorological variables with large geographic gradients.

We used geographic latitude, longitude, and elevation as covariates in the interpolation. Two regions were considered separately: (i) the Spanish Peninsula and Balearic Islands, and (ii) the Canary Islands. Up to 100 neighbouring observatories were used for the interpolation. For semivariogram fitting, when the range was below 20 km or the sill was zero, a spherical model with a nugget effect was imposed.

The interpolated grid layers were validated using a jackknife resampling procedure. This involved sequentially excluding each observatory from the network, estimating the parameter values using interpolation from the remaining stations, and comparing the predicted and observed values. For each gridded distribution parameter (four parameters for each of the two variables analyzed), we computed the Mean Absolute Error (MAE), the Mean Error (ME), and the Relative Standard Deviation (rSD)—a normalized measure expressing the standard deviation relative to the mean. Additionally, we calculated the Kling-Gupta Efficiency (KGE), an error metric combining correlation, bias, and variability, where a value of 1 indicates a perfect match between observed and modelled data. Finally, we computed the Index of Agreement (Willmott et al., 2012), a relative and bounded measure of model performance that retains mean information without being overly influenced by outliers.

2.2.4 Regional assessment at the province level

It is important to emphasize that the occurrence of high-intensity precipitation events exhibits substantial spatial variability, particularly in regions affected by convective rainfall. These events are often characterized by localized maxima and sharp spatial gradients in daily precipitation. However, the same events may have occurred with similar probability in nearby areas. As such, point-based estimates of return periods may lead to an underestimation of the probability of high-impact extreme events at specific locations, and hence misleading assessments of risk. This local underestimation may affect broader areas, creating a false sense of security in the region (García-Ruiz et al. 2000).

To mitigate this issue, in addition to spatial maps, we also calculated magnitude–frequency curves at the provincial level across Spain, which provide estimates the return period of an event of a given magnitude occurring somewhere within the province. Although this approach introduces uncertainties—particularly in provinces with pronounced topographic and climatic gradients—it still offers useful information of return periods for management purposes within administrative boundaries. In essence, it estimates the return period of an event of a given magnitude that occurred at least once somewhere within the province.

To this end, we generated synthetic daily precipitation series for each province, using the highest daily precipitation recorded at any station within the province for each day. These

series were then subjected to a declustering process, and the maximum daily precipitation and the total precipitation magnitude for each event was extracted. A GPD was fitted to these data, and the distribution parameters were calculated for each province.

3 Results

3.1 On-site estimation and validation

The method used to select the threshold for defining precipitation exceedances in the probabilistic analysis yields results comparable to those obtained from most other approaches (Figure S1). Some methods (e.g., Gomes, Himp) produce higher variability between stations and generally higher threshold values, which could introduce substantial spatial inconsistencies and reduce the sample size for reliable probabilistic estimation. In contrast, the 90th percentile of the daily precipitation series (excluding zero values) aligns with the thresholds obtained through other quantitative methods (e.g., Hall, Mindist), and shows only minor differences compared to higher percentiles (92.5th and 95th). Thus, the 90th percentile is a robust and practical choice for threshold selection across Spain. Analysis of mean excess plots confirms this selection. The chosen threshold lies with the range aligns well with the range of values for which confidence intervals begin to widen and the curve deviates from linearity, indicating increased variability (Fig. S2).

Figure 2 shows strong agreement between observed (empirical) CDFs and those modelled using the GPD for maximum daily precipitation recorded during the events at four meteorological stations randomly selected. The model also performs well for the total precipitation over the events (Fig. S3), demonstrating consistency between the two variables. Figure 3 supports these results, summarizing goodness-of-fit tests (Kolmogorov–Smirnov and Anderson–Darling) and agreement statistics (R^2, D and KGE) for the series of maximum precipitation values. The tests confirm that most exceedance series are well described by the GPD, with only a small proportion failing the $p = 0.05$ threshold. Additionally, error/agreement statistics show high concordance between empirical and GPD-modelled distributions, validating the use of exceedance series above the 90th percentile. Similar findings apply to total event precipitation (Figure S4).
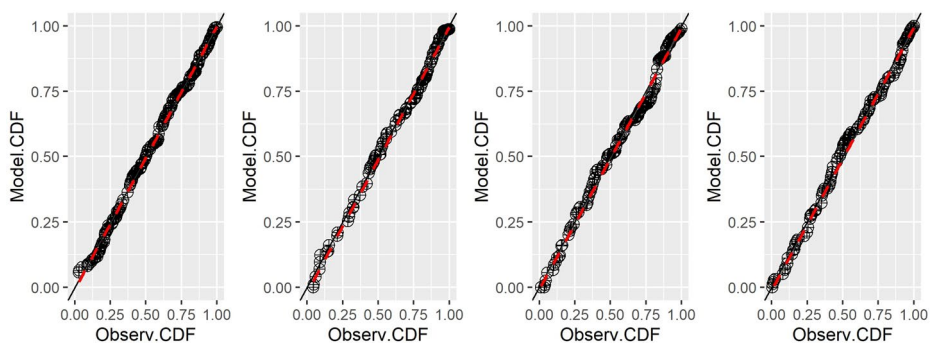

Fig. 2 Relationship between observed and modelled cumulative distribution functions (CDFs) in four meteorological stations randomly selected for the maximum daily precipitation during events
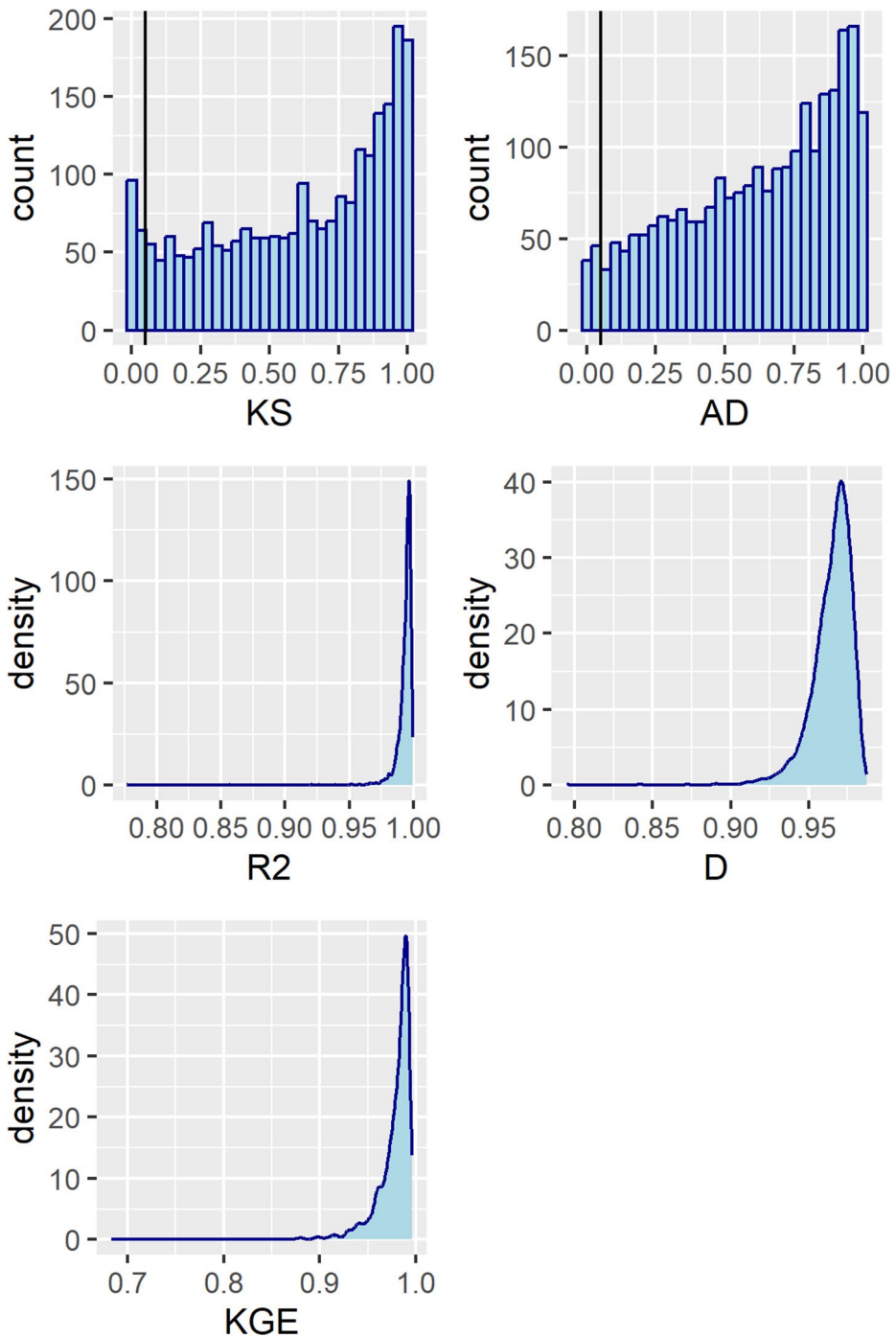
Fig. 3 Goodness of fit tests between observed and modelled CDFs of event's daily maximum precipitation CDFs across all meteorological stations: Kolmogorov–Smirnov, Anderson–Darling, R.^{2}, D and KGE. In K-S and A-D tests vertical limits indicate the limit for statistical significance. The other three statistics show an upper bound at 1

3.2 Parameter mapping

Spatial mapping of GPD parameters derived from point observations reveals strong geographic coherence (Fig. 4). The shape parameter (α) for daily maximum event precipitation shows substantial spatial variability, with the highest values along the Mediterranean coast and some mountain areas. For total event precipitation, the pattern shifts slightly, with maximum α values concentrated in the northwestern Atlantic coast.

Despite their small size, the Canary Islands show significant gradients in α associated with elevation and east–west position. The origin parameter (x_0) displays a similar spatial pattern to α, with some regional differences—e.g., high values in northern Spain for maximum precipitation. The frequency parameter (λ) exhibits a clear north–south gradient, with higher values in the north and lower values in the southeastern Iberian Peninsula (note that the frequency of events is the same for both variables). The scale parameter (κ) shows large spatial variability, but general patterns emerge: a NW–SE gradient for maximum precipitation and a north–south pattern for total event precipitation. In the Canary Islands, κ also shows strong gradients related to elevation and longitude.

Table 1 presents error and agreement statistics (e.g., ME, rSD, r, and d) for each parameter based on a jackknife validation. Overall, α, x_0, and λ show high consistency between observed and predicted values using universal kriging. The Agreement Index D exceeds 0.90 in all cases (except for κ), indicating small differences between station-based estimates and spatial predictions. The κ parameter, however, shows lower accuracy—especially for event's daily maximum precipitation—but still small spatial biases (ME values close to zero). Although predicted values tend to underestimate the range of observations (Fig. S5), the averages and distributions remain similar. At the spatial level there is not a bias in the errors of the parameters comparing the on-site estimated parameters and those parameters interpolated following the jackknife validation. Figures S6 show the spatial pattern of the errors illustrating that the spatial distribution of the errors is randomly distributed as there are not spatial patterns in the distribution of such errors. This is clearly illustrated relating these errors with the geographic coordinates of latitude and longitude (Fig. S7) showing no relationship.

3.3 Precipitation hazard probabilities

Figure 5 illustrates return period curves for both maximum daily precipitation and total event precipitation derived from individual station data. These reveal substantial spatial differences in hazard levels. For instance, while some stations show maximum daily precipitation exceeding 275 mm for a 100-year return period, others are below 70 mm for the same period. Comparable variability is found in total event precipitation estimates.

Return period maps (Fig. 6) clearly reflect spatial gradients. Maximum intensity precipitation during events is highest along coastal areas—particularly the Mediterranean coast—along with the Pyrenean and Cantabrian Mountain ranges, and the central mountain system. In contrast, most inland areas record much lower maximum intensities. For total event precipitation, high values are found in the northwestern, southwestern, and eastern Mediterranean coasts, while inland regions generally show lower totals. Notably, the highest total precipitation values are concentrated in the northwestern Atlantic coast, which is distinct from the pattern seen in maximum intensity. In the Canary Islands, strong spatial contrasts
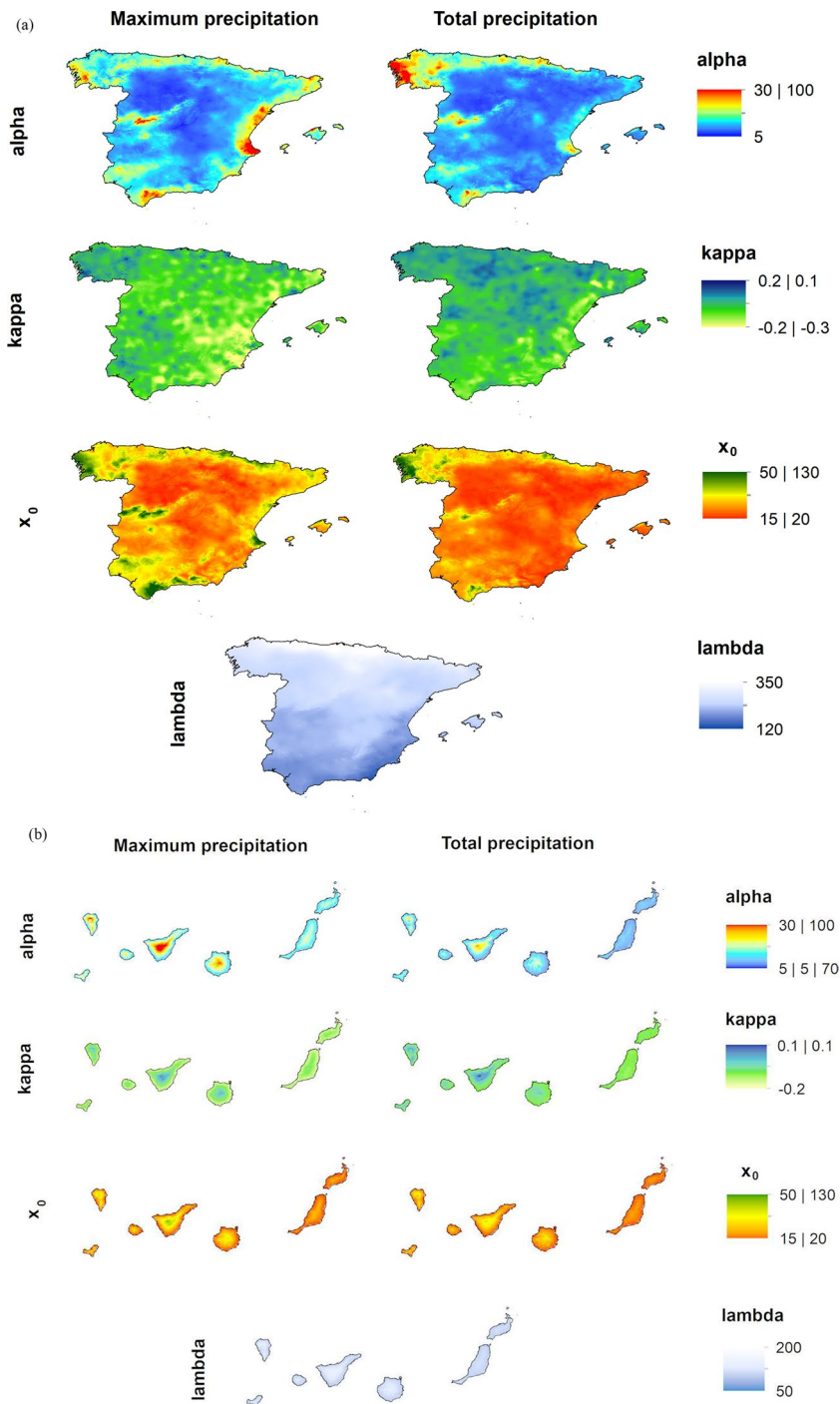
Fig. 4 Spatial distribution of the alpha, kappa, x_0 and lambda parameters corresponding to maximum daily precipitation and total precipitation during extreme precipitation events in **a** Peninsular Spain and the Balearic Islands, and **b** the Canary Islands

Table 1 Cross-validation statistics for the different parameters using the jacknife approach

Daily maximum precipitation	MAE (mm)	ME (mm)	rSD	r	KGE	D
Peninsular Spain and Balearic Islands						
Alpha	2.35	0.06	0.85	0.84	0.78	0.91
Kappa	0.09	0.00	0.60	0.43	0.00	0.61
×0	3.51	−0.02	0.86	0.82	0.78	0.90
Lambda	11.89	0.18	0.97	0.95	0.94	0.98
Total precipitation	MAE (mm)	ME (mm)	rSD	r	KGE	D
Alpha	4.99	0.04	0.91	0.90	0.87	0.95
Kappa	0.06	0.00	0.66	0.55	0.43	0.70
×0	6.53	−0.05	0.91	0.88	0.85	0.94
Lambda	11.89	0.18	0.97	0.95	0.94	0.98
Canary Islands						
Alpha	5.03	−0.26	0.64	0.49	0.37	0.65
Kappa	0.13	0.00	0.59	0.33	0.22	0.54
×0	5.28	−0.08	0.65	0.63	0.51	0.76
Lambda	17.34	1.30	0.93	0.90	0.88	0.95
Total precipitation	MAE (mm)	ME (mm)	rSD	r	KGE	D
Alpha	6.94	−0.24	0.74	0.67	0.58	0.79
Kappa	0.08	0.00	0.59	0.41	0.28	0.61
×0	8.69	1.01	0.69	0.64	0.53	0.76
Lambda	17.34	1.30	0.93	0.90	0.88	0.95

also appear, driven by both island location and elevation. Higher precipitation totals and intensities are concentrated in the highlands of the western islands. The quantiles derived from the parameter maps are consistent with station-level results in Peninsular Spain, the Balearic Islands, and the Canary Islands (Fig. 7, Table S1). Similarly, maps of return periods for events of different magnitude (Figure S8) show important regional differences, with some areas (e.g., central Iberia and easternmost Canary Islands) exhibiting very long return periods—indicating low probabilities of extreme events.

3.4 Regional assessment at the province level

Figure 8 displays the spatial distributions of quantile precipitation for 25- and 50-year return periods, representing the maximum precipitation and total magnitude values expected to occur at least once somewhere in each province. The patterns clearly demonstrate regional disparities in hazard levels, with the highest intensities—exceeding 500 mm in 24 h—occurring in provinces along the eastern Mediterranean coast, and the lowest values in central inland provinces. Magnitude–frequency curves for selected provinces further highlight these contrasts (e.g., the Valencia province in the eastern Mediterranean exhibits extremely high precipitation hazard probabilities compared to inland provinces, Fig. 9). On the contrary, the pattern of the total precipitation recorded during the event shows a different pattern, with the maximum values recorded in some provinces of North and West Spain.
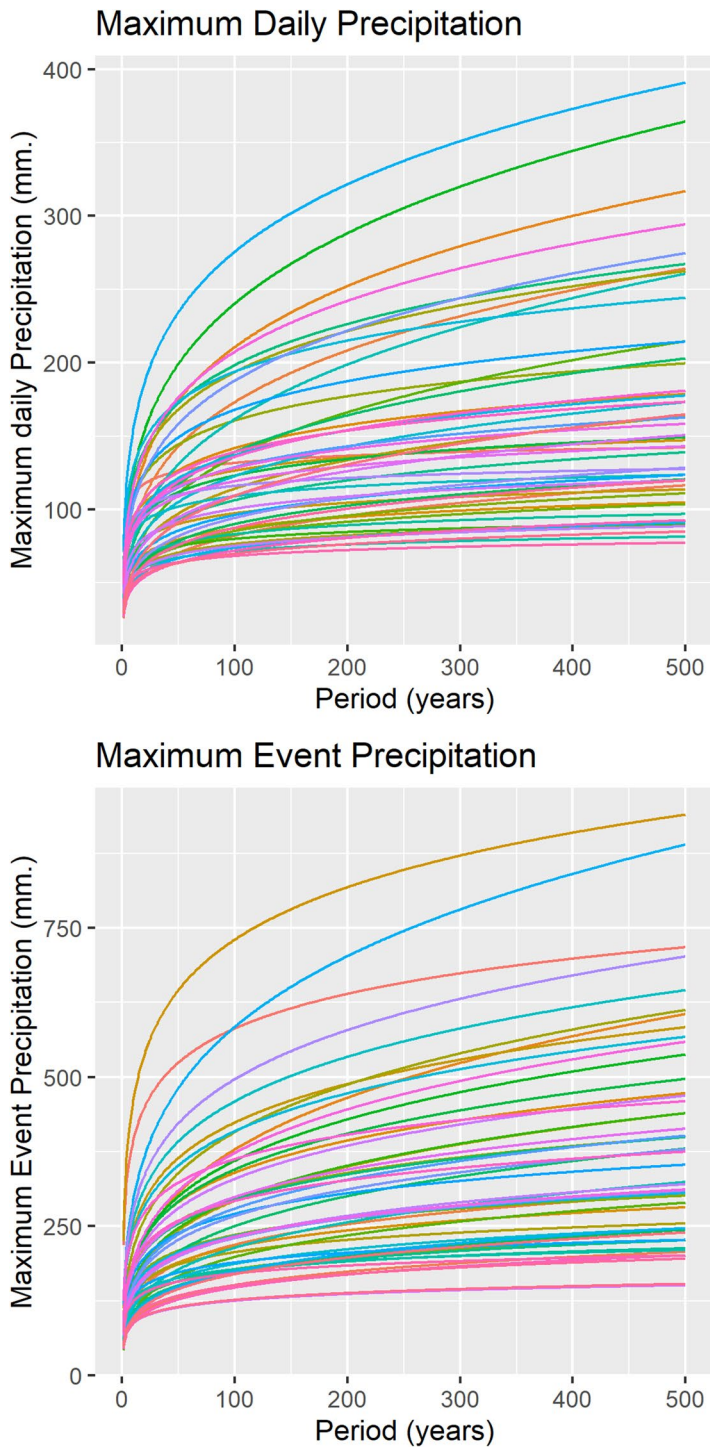
Maximum Daily Precipitation

Maximum Event Precipitation

Fig. 5 Examples of the frequency-magnitude curves from a set of meteorological stations located in different regions of the Iberian Peninsula
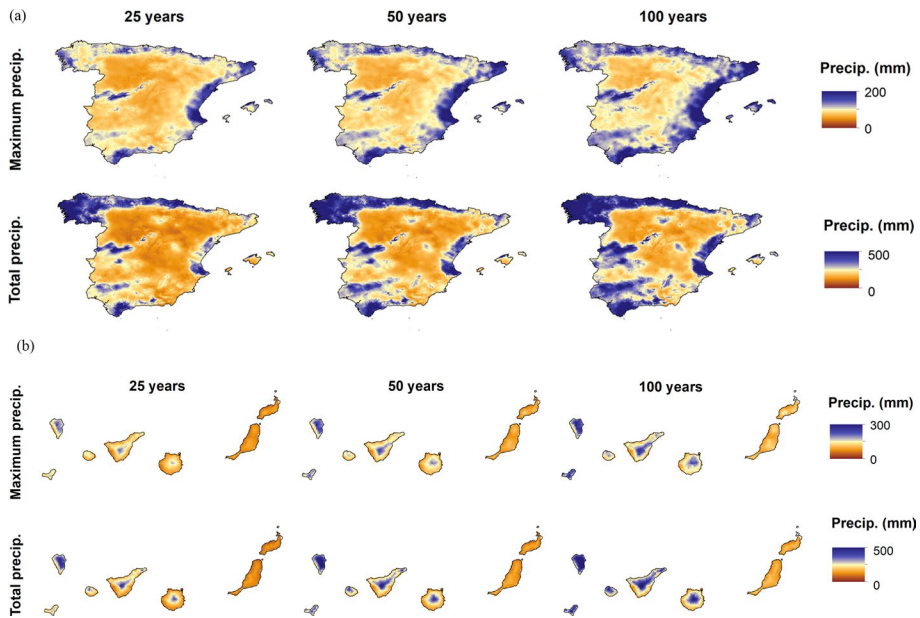
Fig. 6 Quantile estimates for daily maximum daily precipitation and total event precipitation return of 1-in-25, 1-in-50, and 1-in-100 year events (in mm). The Iberian PP and the Balearic Islands are shown at the top, and the Canary Islands at the bottom of the figure

3.5 Integration into extreme precipitation information service

All information generated at the grid cell and provincial scales has been integrated into an interactive climate service (https://retornolluvias.csic.es). The service uses GPD parameters derived for both maximum daily and total event precipitation to calculate return periods for user-selected precipitation thresholds and durations. Users can generate maps based on any desired intensity, magnitude, or return period. Additionally, selecting a specific point or province allows users to generate magnitude–frequency curves for return periods ranging from 1 to 500 years, including associated confidence intervals (Fig. 10). These outputs are downloadable for use in external applications.

4 Discussion and conclusions

This study presents, for the first time, hazard probability maps of extreme precipitation events for Spain. The methodology is grounded in state-of-the-art approaches that estimate the parameters of a probability distribution at individual stations based on long-term daily precipitation records. These parameters are then spatialized into a high-resolution gridded dataset using universal kriging.

Regarding the probability model employed, our results demonstrate that the Generalized Pareto Distribution (GPD) performs well in modelling extreme precipitation quantiles in Spain, aligning with other regional and global assessments of precipitation extremes (Onyutha 2017; Wang et al. 2020). However, mapping high precipitation quantiles is subject
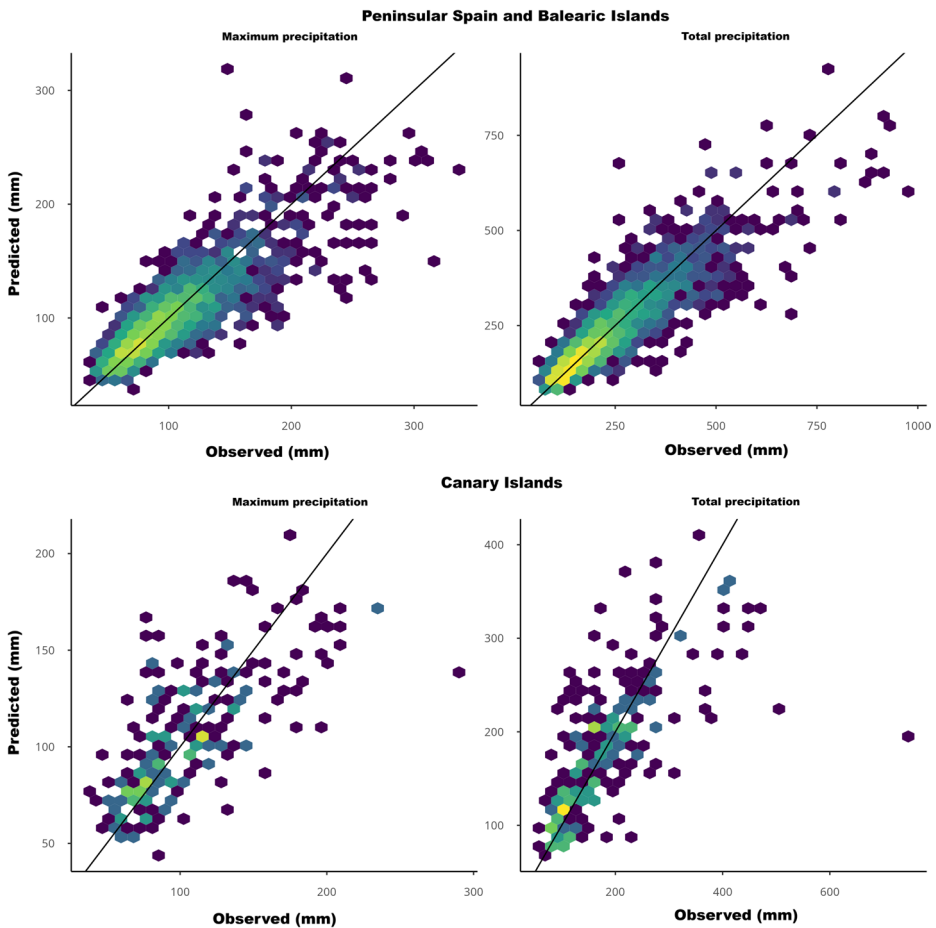
Fig. 7 Cross validation of the daily maximum precipitation (left) and total precipitation (right) expected during events in a 20-year return period, based on on-site calculated parameters and those estimated using the interpolation procedure

to uncertainty in regions with sparse station coverage and complex terrain (Catalini et al. 2021)—features that are prominent across Spain's diverse topography. To address this, we incorporated a high-density observational network and auxiliary elevation data from GIS layers to enhance the interpolation quality in such areas. Using spatial interpolation of distribution parameters—rather than interpolating gridded precipitation estimates directly—offers a more robust approach, as it reduces the expected variance associated with extreme events, consistent with findings from previous studies (Risser et al. 2019). Our results show high agreement between interpolated parameter estimates and, more importantly, between the resulting extreme quantiles and those calculated directly at station level. Achieving this level of consistency in a region like Spain, characterized by highly complex relief and considerable spatial variability in extreme event occurrence, highlights the robustness and utility of the approach adopted.
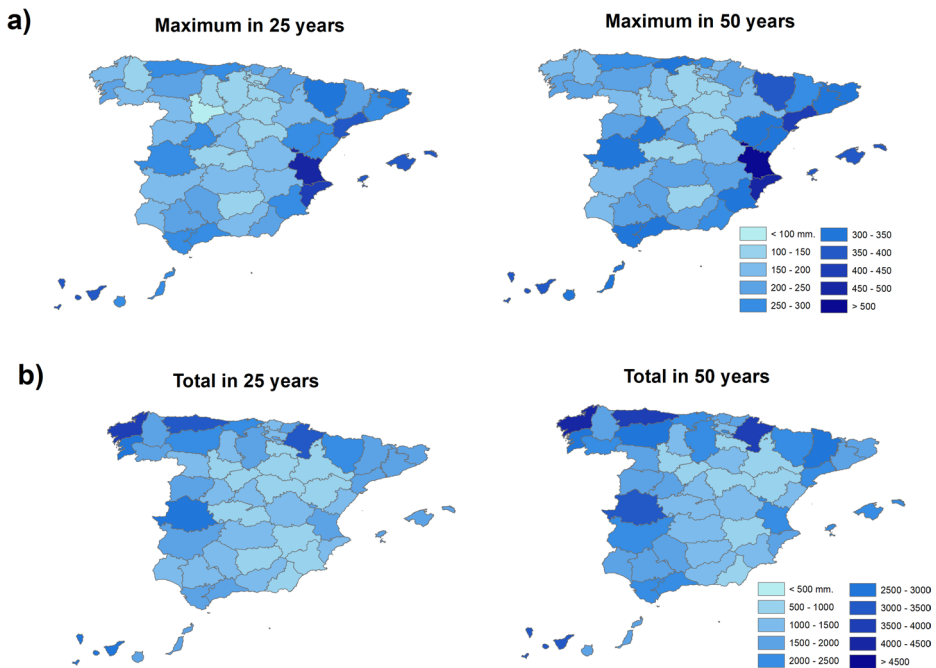
a)

Maximum in 25 years

Maximum in 50 years

< 100 mm.	300 - 350
100 - 150	350 - 400
150 - 200	400 - 450
200 - 250	450 - 500
250 - 300	> 500

b)

Total in 25 years

Total in 50 years

< 500 mm.	2500 - 3000
500 - 1000	3000 - 3500
1000 - 1500	3500 - 4000
1500 - 2000	4000 - 4500
2000 - 2500	> 4500

Fig. 8 Quantile Maps of daily maximum precipitation **a** and total precipitation **b** corresponding to events with return periods of 25 and 50 years, aggregated at the provincial level across Spain

In this study, we applied a stationary approach to estimate the probability of extreme daily precipitation intensities and total event magnitudes. This decision is supported by the observed stationarity of extreme precipitation events in Spain over recent decades (Beguería et al. 2025). Even when trends are present in precipitation series, this does not necessarily justify the adoption of non-stationary models. While some research supports the use of non-stationary models to account for changing climate conditions (Šraj et al. 2016), others argue that stationary models remain more robust and better supported for mapping precipitation hazards (Guerriero et al. 2020; Anzolin et al. 2024). As Serinaldi and Kilsby (2015) argue, non-stationary models, when fitted via inductive inference, introduce structural uncertainty that often outweighs any gain in predictive accuracy. Stationary models, in contrast, offer more coherent and reliable estimates, making them preferable for real-world design and management applications (Luke et al. 2017). It is important to note that under a future non-stationary precipitation regime, the distribution parameters obtained in this study would need to be revisited. Current climate change model simulations for scenarios with increased greenhouse gas concentrations suggest that, as a consequence of thermodynamic processes, extreme precipitation will scale in line with the Clausius–Clapeyron relationship (Brutsaert 2017). However, for the Mediterranean region, these models indicate that a robust increase in the frequency and intensity of heavy rainfall events is only expected under global warming levels exceeding 2 °C (Seneviratne et al. 2021), consistent with more regionally focused studies in Spain (Monjo et al. 2016). Therefore, at least for the coming decades, the stationary approach adopted in this study can be considered a sound basis for generating robust estimates that are useful for assessing extreme precipitation hazards.The observed spatial
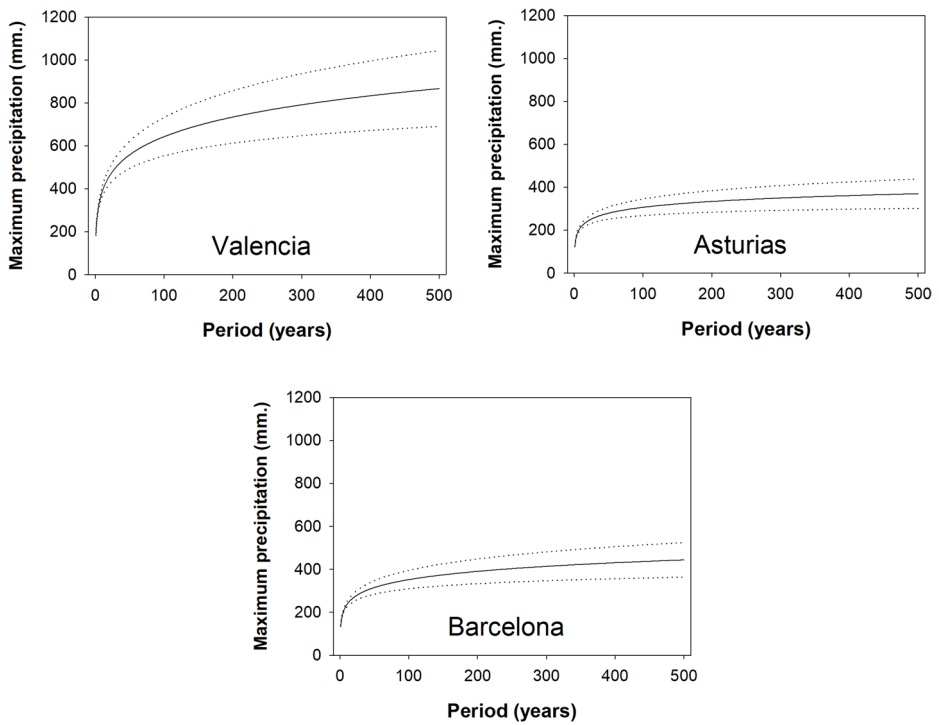
Fig. 9 Examples of magnitude–frequency curves of daily maximum precipitation for three different provinces in Spain
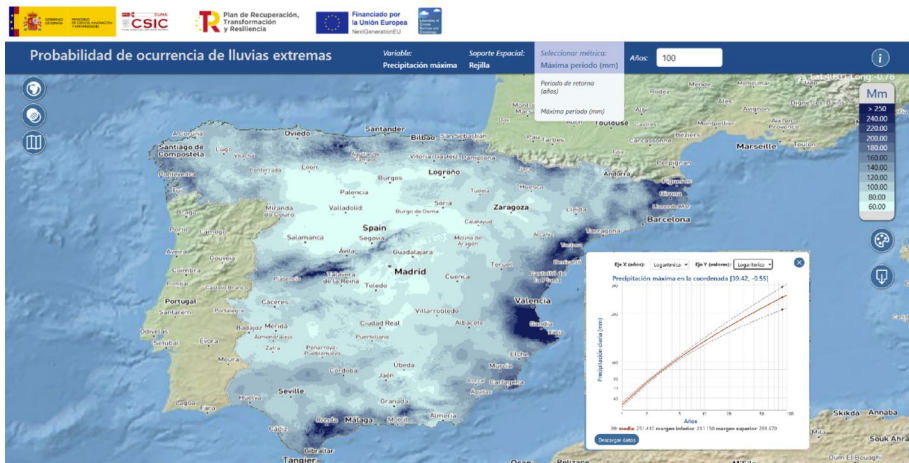

Fig. 10 General structure of the interactive probabilistic extreme precipitation climate service

patterns of daily and event-based precipitation quantiles reflect the underlying climatological dynamics of the country. For instance, high daily precipitation quantiles are predominantly found in eastern and southern Spain near the Mediterranean, largely due to cut-off lows and other convective systems occurring in autumn (Romero et al. 1999; Nieto et al. 2005; Queralt et al. 2009; Pérez-Zanón et al. 2018). In contrast, the highest total precipitation magnitudes during events tend to be recorded in the northwest, linked to westerly flows and low-pressure systems, and in the southwest, where deep cyclones displaced to the south of the Iberian Peninsula induce moist southwesterly flows (Olcina 1994). Overall, the results highlight the contrasting nature of heavy precipitation events across Spain: short, intense convective storms prevail along the Mediterranean coast, while the north is primarily affected by more frequent, longer-lasting, moderate frontal systems linked to extratropical cyclones from the North Atlantic (García-Herrera et al. 2005; Gonzalez-Hidalgo et al. 2025).

The maps of quantiles and return periods for extreme precipitation events in Spain generated in this study are unprecedented at the national scale. While some previous works produced quantile maps for extreme precipitation in specific areas of northeastern Spain (Beguería and Vicente-Serrano 2006; Beguería et al. 2009), they lacked the high spatial resolution required for a robust hazard assessment. At the national level, the only available information was developed by the Spanish Government in 1999 (Ministerio de Fomento 1999). However, those outputs consisted of paper-based isolines generalized over broad regions, which limited their usability. Moreover, the estimations relied on annual maximum precipitation values fitted to a Generalized Extreme Value distribution, a method later shown to be less reliable than approaches based on exceedance series fitted with the Generalized Pareto Distribution (Beguería 2005). This study is not only unprecedented in Spain but also highly novel at the European scale. Several works have analyzed extreme precipitation in Europe from different perspectives, including mapping the frequency of extreme events (Kalbarczyk and Kalbarczyk 2024), providing seasonal probabilistic estimates (Peter et al. 2024), or comparing observed events with model simulations (Beranová and Kyselý 2024). However, only a few studies have produced maps of distribution parameters and high precipitation quantiles, and these have been limited to specific regions (Szolgay et al. 2009; Iliopoulou et al. 2024; Formetta et al. 2024). None have covered such large areas, employed such an extensive network of meteorological stations, or achieved the high spatial resolution presented here. As a result, it is difficult to establish direct comparisons with the magnitude of the precipitation quantiles obtained in this study. Nevertheless, the present work can serve as a methodological reference for improving assessments of precipitation hazard probabilities in Europe and other world regions. Beyond producing high-resolution maps, the study also offers a practical layer of usability by aggregating hazard probabilities at the provincial level. While we did not apply a formal spatial regionalization technique to define homogeneous hazard regions (Haruna et al. 2022; Alshehri et al. 2024), the administrative-level aggregation offers practical utility. It enables authorities to evaluate hazard levels within their jurisdiction, thereby supporting the prioritization of mitigation strategies and resource allocation. This reconciliation between fine-scale hazard estimation and broader governance structures ensures that risk assessments are aligned with administrative and emergency planning frameworks.

The high-resolution maps of return periods for extreme precipitation generated in this study offer a comprehensive view of hydrometeorological extremes in Spain. Their spatial

granularity enables precise estimation of extreme event probabilities, which is particularly valuable for water resource management and agricultural adaptation strategies. In addition to generating accurate, high-resolution probability maps, this study demonstrates their integration into a user-friendly, web-based visualization service. This online platform enhances accessibility to hazard information, allowing users to interactively explore precipitation extremes and improve their situational awareness. The system's capacity for point-specific queries increases its practical value, enabling tailored hazard assessments for individuals and institutions. Such tools support informed, data-driven decision-making and contribute to broader climate resilience initiatives. The integration of high-resolution mapping, province-level summaries, and an interactive online interface provides a comprehensive framework for strengthening Spain's preparedness for extreme precipitation. The new information and interactive tool will support multiple sectors, including water resource management, dam operations, and irrigation planning. They will also enhance civil protection by improving preparedness and response to extreme precipitation events, thereby reducing the associated economic, social, and human impacts. In addition, the tool will contribute to managing related risks such as landslides and debris flows, and will be valuable for infrastructure management, including roads, railways, and drainage systems in urban and industrial areas.

References

Acero FJ, García JA, Gallego MC (2011) Peaks-over-threshold study of trends in extreme rainfall over the Iberian Peninsula. J Clim 24:1089–1105. https://doi.org/10.1175/2010JCLI3627.1

Alshehri M, Mascaro G, Kunkel KE (2024) On the generating mechanisms of daily precipitation in the conterminous united states: climatology, trends, and associated marginal and extreme distributions. J Hydrometeorol 25:1895–1914. https://doi.org/10.1175/JHM-D-24-0024.1

Anzolin G, de Oliveira DY, Vrugt JA, AghaKouchak A, Chaffe PL (2024) Nonstationary frequency analysis of extreme precipitation: Embracing trends in observations. J Hydrol 637:131300

Beguería S (2005) Uncertainties in partial duration series modelling of extremes related to the choice of the threshold value. J Hydrol 303:215–230. https://doi.org/10.1016/j.jhydrol.2004.07.015

Beguería S, Vicente-Serrano SM (2006) Mapping the hazard of extreme rainfall by peaks over threshold extreme value analysis and spatial regression techniques. J Appl Meteorol Climatol 45:108–124. https://doi.org/10.1175/JAM2324.1

Beguería S, Vicente-Serrano SM, López-Moreno JI, García-Ruiz JM (2009) Annual and seasonal mapping of peak intensity, magnitude and duration of extreme precipitation events across a climatic gradient, northeast Spain. Int J Climatol 29:1759–1779. https://doi.org/10.1002/joc.1808

Beguería S, Tomas-Burguera M, Serrano-Notivoli R et al (2019) Gap filling of monthly temperature data and its effect on climatic variability and trends. J Clim 32:7797–7821. https://doi.org/10.1175/JCLI-D-19-0244.1

Beguería S, Tomas-Burguera M, Serrano-Notivoli R et al (2025) Evolution of extreme precipitation in Spain: contribution of atmospheric dynamics and long-term trends. Stoch Env Res Risk Assess. https://doi.org/10.1007/s00477-025-02961-x

Beranová R, Kyselý J (2024) Large-scale heavy precipitation over the Czech Republic and its link to atmospheric circulation in CORDEX regional climate models. Theoret Appl Climatol 155:4737–4748. https://doi.org/10.1007/s00704-024-04907-9

Billios M, Vasiliades L (2024) A network-based clustering method to ensure homogeneity in regional frequency analysis of extreme rainfall. Water 17:38

Braud I, Borga M, Gourley J et al (2016) Flash floods, hydro-geomorphic response and risk management. J Hydrol 541:1–5. https://doi.org/10.1016/j.jhydrol.2016.08.005

Brutsaert W (2017) Global land surface evaporation trend during the past half century: Corroboration by Clausius-Clapeyron scaling. Adv Water Resour 106:3–5. https://doi.org/10.1016/j.advwatres.2016.08.014

Burrough P, McDonnell R (1998) Principle of Geographic Information Systems

Caeiro F, Gomes M (2014) Threshold Selection in Extreme Value Analysis

Catalini CG, Guillen NF, Bazzano FM et al (2021) Web mapping of extreme daily rainfall data in central and Northern Argentina. J Hydrol Eng 26:05021013. https://doi.org/10.1061/(ASCE)HE.1943-5584.0002077

Claps P, Ganora D, Mazzoglio P (2022) Rainfall regionalization techniques. In: Rainfall: Modeling, Measurement and Applications. pp 327–350

Cortesi N, Gonzalez-Hidalgo JC, Brunetti M, de Luis M (2014) Spatial variability of precipitation in Spain. Reg Environ Change 14:1743–1749. https://doi.org/10.1007/s10113-012-0402-6

Das S (2019) Extreme rainfall estimation at ungauged sites: Comparison between region-of-influence approach of regional analysis and spatial interpolation technique. Int J Climatol 39:407–423. https://doi.org/10.1002/joc.5819

Das S, Zhu D, Yin Y (2020) Comparison of mapping approaches for estimating extreme precipitation of any return period at ungauged locations. Stoch Env Res Risk Assess 34:1175–1196. https://doi.org/10.1007/s00477-020-01828-7

Deidda R, Hellies M, Langousis A (2021) A critical analysis of the shortcomings in spatial frequency analysis of rainfall extremes based on homogeneous regions and a comparison with a hierarchical boundaryless approach. Stoch Env Res Risk Assess 35:2605–2628. https://doi.org/10.1007/s00477-021-02008-x

Domínguez-Castro F, Vicente-Serrano SM, Tomás-Burguera M et al (2019) High-spatial-resolution probability maps of drought duration and magnitude across Spain. Nat Hazard 19:611–628. https://doi.org/10.5194/nhess-19-611-2019

Donat MG, Sillmann J, Wild S et al (2014) Consistency of Temperature and Precipitation Extremes across Various Global Gridded In Situ and Reanalysis Datasets*. J Clim 27:5019–5035. https://doi.org/10.1175/JCLI-D-13-00405.1

Ebi KL, Vanos J, Baldwin JW et al (2020) Extreme Weather and Climate Change: Population Health and Health System Implications. Annu Rev Public Health 42:293–315

Formetta G, Dallan E, Borga M, Marra F (2024) Sub-daily precipitation returns levels in ungauged locations: Added value of combining observations with convection permitting simulations. Adv Water Resour 194:104851. https://doi.org/10.1016/j.advwatres.2024.104851

French J, Ing R, Von Allmen S, Wood R (1983) Mortality from flash floods: a review of National Weather Service reports, 1969–81. Public Health Rep 98:584–588

Gamet P, Jalbert J (2022) A flexible extended generalized Pareto distribution for tail estimation. Environmetrics 33:e2744. https://doi.org/10.1002/env.2744

García-Herrera R, Hernández E, Paredes D et al (2005) A MASCOTTE-based characterization of MCSs over Spain, 2000–2002. Atmos Res 73:261–282. https://doi.org/10.1016/j.atmosres.2004.11.003

García-Ruiz JM, Arnáez J, White SM et al (2000) Uncertainty assessment in the prediction of extreme rainfall events: An example from the central Spanish Pyrenees. Hydrol Process 14:887–898. https://doi.org/10.1002/(SICI)1099-1085(20000415)14:5%3c887::AID-HYP976%3e3.0.CO;2-0

Gonzalez-Hidalgo JC, Beguería S, Peña-Angulo D, Blanco VT (2025) Catalogue and analysis of extraordinary precipitation events in the Spanish Mainland, 1916–2022. Int J Climatol 45:e8785. https://doi.org/10.1002/joc.8785

Guerriero L, Ruzza G, Guadagno FM, Revellino P (2020) Flood hazard mapping incorporating multiple probability models. J Hydrol 587:125020. https://doi.org/10.1016/j.jhydrol.2020.125020

Hall P, Welsh A (1985) Adaptive estimates of parameters of regular variation. Annals Stat. https://doi.org/10.1214/aos/1176346596

Haruna A, Blanchet J, Favre A-C (2022) Performance-based comparison of regionalization methods to improve the at-site estimates of daily precipitation. Hydrol Earth Syst Sci 26:2797–2811. https://doi.org/10.5194/hess-26-2797-2022

Hershfield DM (1973) on the probability of extreme rainfall events. Bull Am Meteor Soc 54:1013–1018. https://doi.org/10.1175/1520-0477(1973)054%3c1013:OTPOER%3e2.0.CO;2

Hosking JRM, Wallis JR (1987) Parameter and quantile estimation for the generalized Pareto distribution. Technometrics 29:339–349. https://doi.org/10.1080/00401706.1987.10488243

Iliopoulou T, Koutsoyiannis D, Malamos N et al (2024) A stochastic framework for rainfall intensity–time scale–return period relationships. Part II: point modelling and regionalization over Greece. Hydrol Sci J 69:1092–1112. https://doi.org/10.1080/02626667.2024.2345814

Jonkman SN (2005) Global perspectives on loss of human life caused by floods. Nat Hazards 34:151–175

Kalbarczyk R, Kalbarczyk E (2024) Risk of natural hazards caused by extreme precipitation in Poland in 1951–2020. Water. https://doi.org/10.3390/w16121705

Khalili D, Farnoud T, Jamshidi H et al (2011) Comparability analyses of the SPI and RDI meteorological drought indices in different climatic zones. Water Resour Manage 25:1737–1757. https://doi.org/10.1007/s11269-010-9772-z

Kirschbaum D, Adler R, Adler D et al (2012) Global distribution of extreme precipitation and high-impact landslides in 2010 relative to previous years. J Hydrometeorol 13:1536–1551. https://doi.org/10.1175/JHM-D-12-02.1

Kirschbaum D, Kapnick SB, Stanley T, Pascale S (2020) Changes in Extreme precipitation and landslides over high mountain Asia. Geophys Res Lett. https://doi.org/10.1029/2019GL085347

Koutsoyiannis D, Iliopoulou T, Koukouvinos A, Malamos N (2024) A stochastic framework for rainfall intensity–time scale–return period relationships. Part I: theory and estimation strategies. Hydrol Sci J 69:1082–1091. https://doi.org/10.1080/02626667.2024.2345813

Lesk C, Rowhani P, Ramankutty N (2016) Influence of extreme weather disasters on global crop production. Nature 529:84–87

Li C, Zwiers F, Zhang X et al (2021) Changes in annual extremes of daily temperature and precipitation in CMIP6 models. J Clim 34:3441–3460. https://doi.org/10.1175/JCLI-D-19-1013.1

Luke A, Vrugt JA, AghaKouchak A et al (2017) Predicting nonstationary flood frequencies: Evidence supports an updated stationarity thesis in the United States. Water Resour Res 53:5469–5494. https://doi.org/10.1002/2016WR019676

Mascaro G (2018) On the distributions of annual and seasonal daily rainfall extremes in central Arizona and their spatial variability. J Hydrol 559:266–281. https://doi.org/10.1016/j.jhydrol.2018.02.011

Meddi M, Toumi S (2015) Spatial variability and cartography of maximum annual daily rainfall under different return periods in Northern Algeria. J Mt Sci 12:1403–1421. https://doi.org/10.1007/s11629-014-3084-3

Merz B, Kreibich H, Schwarze R, Thieken A (2010) Review article "assessment of economic flood damage." Natural Hazards and Earth System Science 10:1697–1724

Milojevic T, Blanchet J, Lehning M (2023) Determining return levels of extreme daily precipitation, reservoir inflow, and dry spells. Front Water. https://doi.org/10.3389/frwa.2023.1141786

Ministerio de Fomento (1999) Máximas lluvias diarias en la España Peninsular. Ministerio de Fomento

Miniussi A, Marra F (2021) Estimation of extreme daily precipitation return levels at-site and in ungauged locations using the simplified MEV approach. J Hydrol 603:126946. https://doi.org/10.1016/j.jhydrol.2021.126946

Monjo R, Gaitán E, Pórtoles J et al (2016) Changes in extreme precipitation over Spain using statistical downscaling of CMIP5 projections. Int J Climatol 36:757–769. https://doi.org/10.1002/joc.4380

Mulligan M (1998) Modelling the geomorphological impact of climatic variability and extreme events in a semi-arid environment. Geomorphology 24:59–78. https://doi.org/10.1016/S0169-555X(97)00101-3

Myhre G, Alterskjær K, Stjern CW et al (2019) Frequency of extreme precipitation increases extensively with event rareness under global warming. Sci Rep 9:16063. https://doi.org/10.1038/s41598-019-52277-4

Nerantzaki SD, Papalexiou SM (2022) Assessing extremes in hydroclimatology: a review on probabilistic methods. J Hydrol 605:127302. https://doi.org/10.1016/j.jhydrol.2021.127302

Nieto R, Gimeno L, de la Torre L et al (2005) Climatological features of cutoff low systems in the Northern Hemisphere. J Clim 18:3085–3103. https://doi.org/10.1175/JCLI3386.1

Norbiato D, Borga M, Sangati M, Zanon F (2007) Regional frequency analysis of extreme precipitation in the eastern Italian Alps and the August 29, 2003 flash flood. J Hydrol 345:149–166. https://doi.org/10.1016/j.jhydrol.2007.07.009

Olcina J (1994) Riesgos climáticos en la Península Ibérica. Phentalon

Onyutha C (2017) On rigorous drought assessment using daily time scale: non-stationary frequency analyses, revisited concepts, and a new method to yield non-parametric indices. Hydrology. https://doi.org/10.3390/hydrology4040048

Papalexiou SM, Montanari A (2019) Global and regional increase of precipitation extremes under global warming. Water Resour Res 55:4901–4914. https://doi.org/10.1029/2018WR024067

Pebesma EJ (2004) Multivariable geostatistics in S: the gstat package. Comput Geosci 30:683–691. https://doi.org/10.1016/j.cageo.2004.03.012

Peng M, Zhang L (2012) Analysis of human risks due to dam-break floods-part 1: a new model based on Bayesian networks. Nat Hazards 64:903–933. https://doi.org/10.1007/s11069-012-0275-5

Pérez-Zanón N, Casas-Castillo MC, Peña JC et al (2018) Analysis of synoptic patterns in relationship with severe rainfall events in the Ebre Observatory (Catalonia). Acta Geophys 66:405–414. https://doi.org/10.1007/s11600-018-0126-1

Peter M, Rust HW, Ulbrich U (2024) Interannual variations in the seasonal cycle of extreme precipitation in Germany and the response to climate change. Nat Hazard 24:1261–1285. https://doi.org/10.5194/nhess-24-1261-2024

Pickands III J (1975) Statistical inference using extreme order statistics. Annals Stat 3:119–131. https://doi.org/10.1214/aos/1176343003

Queralt S, Hernández E, Barriopedro D et al (2009) North Atlantic Oscillation influence and weather types associated with winter total and extreme precipitation events in Spain. Atmos Res 94:675–683. https://doi.org/10.1016/j.atmosres.2009.09.005

Rao R, Hamed K (2000) Flood Frequency Analysis. CRC

Risser MD, Paciorek CJ, Wehner MF et al (2019) A probabilistic gridded product for daily precipitation extremes over the United States. Clim Dyn 53:2517–2538. https://doi.org/10.1007/s00382-019-04636-0

Romero R, Ramis C, Guijarro JA (1999) Daily rainfall patterns in the Spanish Mediterranean area: an objective classification. Int J Climatol 19:95–112. https://doi.org/10.1002/(SICI)1097-0088(199901)19:1%3c95::AID-JOC344%3e3.0.CO;2-S

Seneviratne SI, Zhang X, Adnan M, et al (2021) Weather and Climate Extreme Events in a Changing Climate. Climate Change 2021: The Physical Science Basis. Contribution of Working Group I to the Sixth Assessment Report of the Intergovernmental Panel on Climate Change

Serinaldi F, Kilsby CG (2014) Rainfall extremes: Toward reconciliation after the battle of distributions. Water Resour Res 50:336–352. https://doi.org/10.1002/2013WR014211

Serinaldi F, Kilsby CG (2015) Stationarity is undead: uncertainty dominates the distribution of extremes. Adv Water Resour 77:17–36. https://doi.org/10.1016/j.advwatres.2014.12.013

Serrano-Notivoli R, Beguería S, Saz MÁ, de Luis M (2018) Recent trends reveal decreasing intensity of daily precipitation in Spain. Int J Climatol 38:4211–4224. https://doi.org/10.1002/joc.5562

Singh P, Sinha VSP, Vijhani A, Pahuja N (2018) Vulnerability assessment of urban road network from urban flood. Int J f Disaster Risk Reduct 28:237–250. https://doi.org/10.1016/j.ijdrr.2018.03.017

Smith JA, Baeck ML, Yang L et al (2019) The paroxysmal precipitation of the desert: flash floods in the Southwestern United States. Water Resour Res 55:10218–10247. https://doi.org/10.1029/2019WR025480

Šraj M, Viglione A, Parajka J, Blöschl G (2016) The influence of non-stationarity in extreme hydrological events on flood frequency estimation. J Hydrol Hydromech 64:426–437. https://doi.org/10.1515/johh-2016-0032

Szolgay J, Parajka J, Kohnová S, Hlavčová K (2009) Comparison of mapping approaches of design annual maximum daily precipitation. Atmos Res 92:289–307. https://doi.org/10.1016/j.atmosres.2009.01.009

Tarasova L, Merz R, Kiss A, et al (2019) Causative classification of river flood events. Wiley Interdisciplinary Reviews: Water

Ul Hassan M, Noreen Z, Ahmed R (2021) Regional frequency analysis of annual daily rainfall maxima in Skåne, Sweden. Int J Climatol 41:4307–4320. https://doi.org/10.1002/joc.7074

Vicente-Serrano SM, Beguería S, López-Moreno JI et al (2010) A complete daily precipitation database for northeast Spain: reconstruction, quality control, and homogeneity. Int J Climatol 30:1146–1163. https://doi.org/10.1002/joc.1850

Vicente-Serrano SM, Tramblay Y, Reig F et al (2025) High temporal variability not trend dominates Mediterranean precipitation. Nature 639:658–666. https://doi.org/10.1038/s41586-024-08576-6

Wang Z, Wen X, Lei X et al (2020) Effects of different statistical distribution and threshold criteria in extreme precipitation modelling over global land areas. Int J Climatol 40:1838–1850. https://doi.org/10.1002/joc.6305

Willmott CJ, Robeson SM, Matsuura K (2012) A refined index of model performance. Int J Climatol 32(13):2088–2094

Yao Y, Liu J, Wang Z et al (2020) Responses of soil aggregate stability, erodibility and nutrient enrichment to simulated extreme heavy rainfall. Sci Tot Environ. https://doi.org/10.1016/j.scitotenv.2019.136150

Yin S, Wang Z, Zhu Z et al (2018) Using Kriging with a heterogeneous measurement error to improve the accuracy of extreme precipitation return level estimation. J Hydrol 562:518–529. https://doi.org/10.1016/j.jhydrol.2018.04.064

Zou W, Yin S, Wang W (2021) Spatial interpolation of the extreme hourly precipitation at different return levels in the Haihe River basin. J Hydrol 598:126273. https://doi.org/10.1016/j.jhydrol.2021.126273

Authors and Affiliations

S. M. Vicente-Serrano[1,2] [iD] · **S. Beguería[3,2]** · **F. Reig[1,2]** · **A. Royo[1,2]** · **M. Arretxea[4]** · **M. Gil[3,2]** · **B. Latorre[3,2]** · **A. El Kenawy[1,2]** · **M. Franquesa[1,2]** · **A. Halifa-Marin[1,2]** · **M. Adell-Michavila[1,2]** · **A. Crespillo[1,2]** · **D. Pérez-Pajuelo[1,2]** · **F. Domínguez-Castro[1,2]** · **D. Barriopedro[4]** · **J. M. Gutiérrez[5]** · **C. Azorin-Molina[6]** · **L. Gimeno[7,8,9]** · **R. Nieto[7,8,9]**

✉ S. M. Vicente-Serrano
  svicen@ipe.csic.es

1   Instituto Pirenaico de Ecología, IPE-CSIC, Zaragoza, Spain

2   Laboratorio de Climatologia y Servicios Climaticos (LCSC), CSIC–Universidad de Zaragoza, Zaragoza, Spain

3   Estación Experimental de Aula Dei, EEAD-CSIC, Zaragoza, Spain

4   Instituto de Geociencias (IGEO-CSIC-UCM), Madrid, Spain

5   Instituto de Fisica de Cantabria , IFCA-CSIC - Universidad de Cantabria, Santander, Spain

6   Centro de Investigaciones Sobre Desertificación, Consejo Superior de Investigaciones Científicas (CIDE, Climate, Atmosphere and Ocean Laboratory (Climatoc-Lab), CSIC-UV-Generalitat Valenciana), Moncada, Valencia, Spain

7   Environmental Physics Laboratory (EPhysLab), CIM-UVigo, Universidade de Vigo, Ourense, Spain

8   Unidad Asociada CSIC-Universidad de Vigo: Grupo de Física de La Atmosfera y del Océano, Pontevedra, Spain

9   Galicia Supercomputing Center (CESGA), Santiago de Compostela, Spain